Journal of Power Sources 195 (2010) 280–284

Contents lists available at ScienceDirect

Journal of Power Sources

journal homepage: www.elsevier.com/locate/jpowsour

Short communication

Co-free, iron perovskites as cathode materials for intermediate-temperature solid oxide fuel cells

Shu-en Hou[a,c], José Antonio Alonso[b,c,*], John B. Goodenough[c]

[a] Engineering Research Center of Nano-Geo Materials of Ministry of Education, China University of Geosciences, Wuhan, 430074, China
[b] Instituto de Ciencia de Materiales de Madrid, CSIC, Cantoblanco, E-28049 Madrid, Spain
[c] Texas Materials Institute, ETC 9.102, The University of Texas at Austin, Austin, TX 78712, USA

ARTICLE INFO

Article history:
Received 25 April 2009
Received in revised form 3 June 2009
Accepted 9 July 2009
Available online 18 July 2009

Keywords:
Intermediate-temperature SOFC
Co-free cathode
MIEC oxide
$SrFeO_3$
Hydrogen

ABSTRACT

We have developed a Co-free solid oxide fuel cell (SOFC) based upon Fe mixed oxides that gives an extraordinary performance in test-cells with H_2 as fuel. As cathode material, the perovskite $Sr_{0.9}K_{0.1}FeO_{3-\delta}$ (SKFO) has been selected since it has an excellent ionic and electronic conductivity and long-term stability under oxidizing conditions; the characterization of this material included X-ray diffraction (XRD), thermal analysis, scanning microscopy and conductivity measurements. The electrodes were supported on a 300-μm thick pellet of the electrolyte $La_{0.8}Sr_{0.2}Ga_{0.83}Mg_{0.17}O_{3-\delta}$ (LSGM) with Sr_2MgMoO_6 as the anode and SKFO as the cathode. The test cells gave a maximum power density of 680 mW cm^{-2} at 800 °C and 850 mW cm^{-2} at 850 °C, with pure H_2 as fuel. The electronic conductivity shows a change of regime at $T \approx 350$ °C that could correspond to the phase transition from tetragonal to cubic symmetry. The high-temperature regime is characterized by a metallic-like behavior. At 800 °C the crystal structure contains 0.20(1) oxygen vacancies per formula unit randomly distributed over the oxygen sites (if a cubic symmetry is assumed). The presence of disordered vacancies could account, by itself, for the oxide-ion conductivity that is required for the mass transport across the cathode. The result is a competitive cathode material containing no cobalt that meets the target for the intermediate-temperature SOFC.

1. Introduction

The SOFC is attractive in concept for generation of off-grid, distributed electric power or for a bottoming cycle of a conventional power plant. However, the manufacture at a competitive cost of a product that has sufficient life, power output, and reliability at an operating temperature $T_{op} \approx 800$ °C remains a challenge. Both the cathode and the anode materials need improvement to reduce energy losses due to the electrode polarization. For instance, for the standard cathode material $La_{1-x}A_xMnO_{3+\delta}$, the activation polarization is too large at $T_{op} < 800$ °C.

A good cathode material requires a mixed ionic–electronic conductor (MIEC) that has a thermal expansion matched to that of the electrolyte and contains mobile oxygen vacancies. To date, the search for new materials has concentrated on transition-metal oxides having an active redox couple pinned at the top of the O 2p bands, *i.e.*, Fe(IV)/Fe(III), Co(IV)/Co(III), Ni(III)/Ni(II), Ni(IV)/Ni(III), and Cu(III)/Cu(II). Good oxygen-vacancy mobility in the oxoperovskites has led to extensive investigation of $LaFeO_3$, $LaCoO_3$, and/or $LaNiO_3$ perovskites doped with Sr or Ca. The best of these MIEC cathodes has been $La_{1-x}Sr_xFe_{1-y}Co_yO_{3-\delta}$ with x and y chosen to give the largest δ at T_{op} compatible with an acceptable match of the thermal expansion to that of the electrolyte [1,2]. On the other hand, it is well known that $SrFeO_x$ [3–6] and other perovskites based on the $SrFe_yCo_{1-y}O_x$ ($0 \le y \le 1.0$; $2.5 \le x \le 3.0$) system [7] are MIECs in which the reversible oxygen non-stoichiometry may be exploited for gas-sensor applications and in energy-conversion devices. These materials undergo reversible phase transitions from the conductive cubic perovskite structure to the much less conductive brownmillerite structure. The Co(IV)/Co(III) couple has given the lowest activation polarization loss, but cobalt is too expensive even when diluted with iron to reduce the thermal expansion associated with low-spin to higher spin transitions on the Co(III) ions. The development of a Co-free cathode based upon the $SrFeO_x$ system that combines the adequate electronic and oxide-ion conductivity properties was our goal in this work.

Concerning the anode, double perovskites of the type $Sr_2BB'O_6$, in particular Sr_2MgMoO_6 [8,9], have been demonstrated to be an excellent alternative to the standard cermets (Ni + YSZ) and to have an excellent performance in single cells in hydrogen and methane, so Sr_2MgMoO_6 has been the anode utilized in this work.

* Corresponding author at: Instituto de Ciencia de Materiales de Madrid, CSIC, Cantoblanco, E-28049 Madrid, Spain.
E-mail address: ja.alonso@icmm.csic.es (J.A. Alonso).

0378-7753/$ – see front matter © 2009 Elsevier B.V. All rights reserved.
doi:10.1016/j.jpowsour.2009.07.017

2. Experimental

$Sr_{0.9}K_{0.1}FeO_{3-\delta}$ material was obtained in polycrystalline form by a standard ceramic procedure. Stoichiometric amounts of analytical grade $Sr(CH_3COO)_2$, $K_2C_2O_4{\cdot}H_2O$ and $Fe(NO_3)_9{\cdot}H_2O$ were heated in air in alumina crucibles at 900 °C for 15 h, 1000 °C for 15 h and 1100 °C for 10 h with intermediate grindings, followed by ball milling for 40 min. The reaction products were characterized by powder X-ray diffraction (XRD) for phase identification and to asses phase purity. The characterization was performed with a Philips X-pert diffractometer (40 kV, 30 mA) in Bragg–Brentano reflection geometry with Cu Kα radiation (λ = 1.5418 Å). The XRD patterns were analysed by the Rietveld method [10] with the Fullprof program [11]. A pseudo-Voigt function was considered to generate the profile shape. The background was fit to a 5th degree polynomial.

The electrical conductivity measurements were performed from 200 to 900 °C in air with a *dc* four-probe method. For this purpose, a cylindrical pellet of 6.5 mm diameter and 10.2 mm length was sintered at 1200 °C for 10 h. Pt wire and Pt paste were used to make the four probes. A current load of 10–100 mA was applied and the potential drop was recorded in an EG&G Princeton Applied Research Potentiostat–Galvanostat, model 273.

Thermogravimetric (TG) curves in air were obtained in a PerkinElmer TG7 apparatus in the temperature range 42–824 °C, with a heating and cooling speed of 3 °C min^{-1} and an intermediate isothermal heating at 824 °C for 1 h before starting the cooling run. About 50 mg of sample was used.

Single-cell tests were made on electrolyte-supported cells with $La_{0.8}Sr_{0.2}Ga_{0.83}Mg_{0.17}O_{3-\delta}$ (LSGM) as the electrolyte. LSGM pellets of 20-mm diameter were sintered at 1450° C for 20 h and then polished with a diamond wheel to a thickness of 300 μm. The anode was the double perovskite $Sr_2MgMoO_{6-\delta}$ (SMMO) prepared by a sol–gel technique as described elsewhere [8]; $La_{0.4}Ce_{0.6}O_{2-\delta}$ (LDC) was used as a buffer layer between the anode and the electrolyte in order to prevent the interdiffusion of ionic species between perovskite and electrolyte. Inks of LDC, SMMO and SKFO were prepared with a binder (V-006 from Heraeus). LDC ink was screen-printed onto one side of the LSGM disk followed by a thermal treatment at 1300 °C in air for 1 h. SMMO was subsequently screen printed onto the LDC layer and fired at 1275 °C in air. SKFO was finally screen-printed onto the other side of the disk and fired at 1100 °C for 1 h. The working electrode area of the cell was 0.24 cm^2 (0.6 cm × 0.4 cm). Reference electrodes of the same materials as the working electrodes were used to monitor the overpotentials of the cathode and anode in the cell configuration (see Fig. 4). Pt gauze with a small amount of Pt paste in separate dots was used as current collector at both the anodic and the cathodic sides for ensuring electrical contact. The cells were tested in a vertical tubular furnace at 750, 800 and 850 °C; the anode side was fed with a flow of pure H_2 (20 ml min^{-1}) whereas the cathode worked in an air flow of 100 ml min^{-1}.

Micrographs of cross-sectional layers of the SKFO/LSGM/LDC/SMMO cells were taken with a scanning electron microscope (SEM, JEOL JSM-5610).

3. Results and discussion

A $Sr_{0.9}K_{0.1}FeO_{3-\delta}$ sample was obtained as a polycrystalline perovskite, black in color. Fig. 1 shows the room-temperature XRD pattern. The crystal structure of the main perovskite phase can be refined from the XRD data in a tetragonal unit cell consisting of a slight axial deformation of the perovskite aristotype with $a = b = 3.86062(3)$ Å and $c = 3.87316(5)$ Å. It is defined in the *P*4/*mmm* space group with Sr and K distributed at random over the 1*d* (1/2 1/2 1/2) positions, Fe at 1*a* (0 0 0) sites, and O1 and O2 oxygen atoms at 2*f* (0 1/2 0) and 1*b* (0 0 1/2) positions, respectively. The

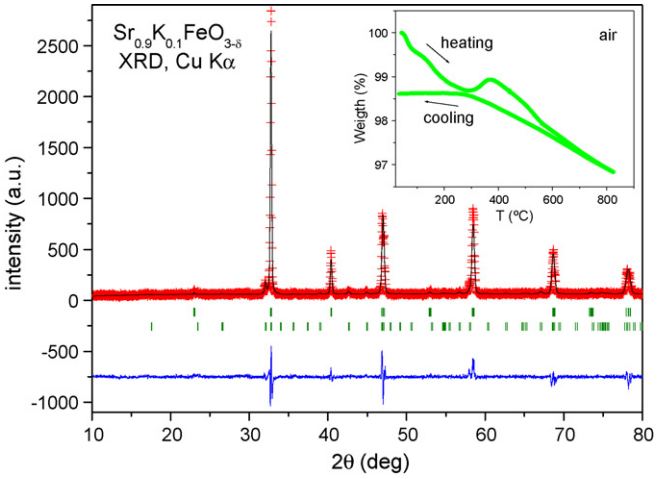

Fig. 1. XRD Rietveld profiles of $Sr_{0.9}K_{0.1}FeO_{3-\delta}$, defined in the *P*4/*mmm* space group. The first and second series of vertical bars are the allowed Bragg reflections for the main perovskite phase and the minor impurity $Sr_3Fe_2O_{6.75}$, respectively. The inset shows the TG curve, recorded in air in the heating and cooling runs.

refinement of the oxygen occupancy factors leads to a crystallographic stoichiometry $Sr_{0.9}K_{0.1}FeO_{2.96(4)}$ at room temperature. The nominal oxidation state for Fe is 4.02(8)+. Fig. 1 illustrates the goodness of the fit, with discrepancy factors $R_{Bragg} = 8.32\%$, $\chi^2 = 2.15$. The presence of a minor impurity identified as $Sr_3Fe_2O_{6.75}$ was taken into account and its crystal structure was introduced as a second phase in the refinement (space group *I*4/*mmm* [12]). From the scale factors of the main perovskite and the impurity, the relative amount of $Sr_3Fe_2O_{6.75}$ was determined to be 6.6(6)%. The inset of Fig. 1 shows the thermogravimetric curves obtained in the heating and cooling runs in an air atmosphere. The initial weight losses observed between 40 and 290 °C are due to water from humid air, and the gain observed below 370 °C can be considered to be a partial oxidation or carbonization of the sample in the heating run, which reverses at higher temperatures. These features are not observed in the cooling run where a monotonic weight gain is observed above 280 °C. From the difference between the final weight at room temperature and the one observed at 800 °C, we can assign an oxygen content of 2.80(1) to the perovskite oxide at the typical working temperature of the cathode material in the fuel cell. This corresponds to an oxidation state of 3.70(2)+ for Fe in $Sr_{0.9}K_{0.1}FeO_{2.80(1)}$.

The inset of Fig. 2 shows the thermal variation of the electronic conductivity σ of $Sr_{0.9}K_{0.1}FeO_{3-\delta}$ from 200 to 900 °C in air atmosphere. A mixed-valent Fe(III)/Fe(IV) couple can provide a good electronic conduction. Fig. 2 shows the plot of $\ln(\sigma T)$ *vs* $1/T$, which displays no linear regions, but a continuous evolution from a polaronic mechanism to a metallic behavior, characterized by a positive slope, from temperatures above ≈350 °C. It is noteworthy that at 800 °C in air, the conductivity still exhibits the relatively high value of $\sigma \approx 26$ S cm^{-1}.

Fig. 3 shows the cell voltage and power density as a function of the current density at three different temperatures for the single fuel cell built with $Sr_{0.9}K_{0.1}FeO_{3-\delta}$ as cathode and Sr_2MgMoO_6 as anode, both supported on a 300-μm thick LSGM electrolyte, working in a pure H_2 flow. The inset of Fig. 4 shows the configuration of the electrolyte-supported test cell (cathodic side). The maximum power density obtained at 850 °C is 850 mW cm^{-2}, 680 mW cm^{-2} at 800 °C and 520 mW cm^{-2} at 750 °C. To test the stability of the cathode, we ran the cells for repeated power cycles from open-circuit voltage (OCV) to 0.4 V and back to OCV. Each power cycle lasted 20 min. Fig. 4 illustrates a measure of P_{max} of the single cell at 800 °C against the cycle number; P_{max} did not drop significantly after 50 cycles. The anode and cathode overpotentials, η_a and η_c, of

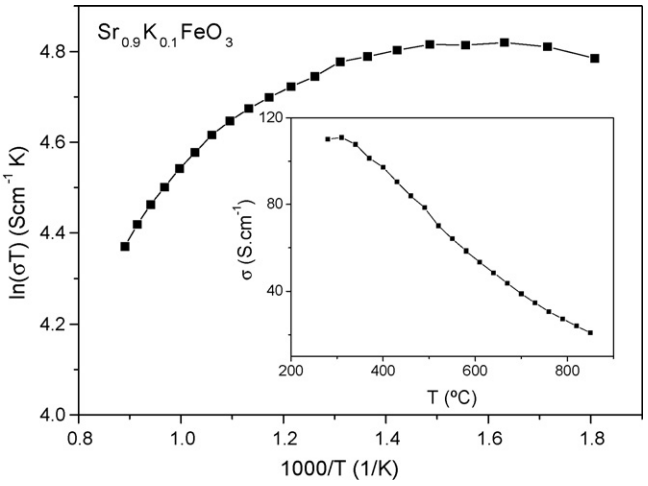

Fig. 2. Ln(σT) *vs* 1000/T plot of the electrical conductivity of $Sr_{0.9}K_{0.1}FeO_{3-\delta}$ measured in air in the 200–900 °C temperature range. The inset shows the thermal variation of σ.

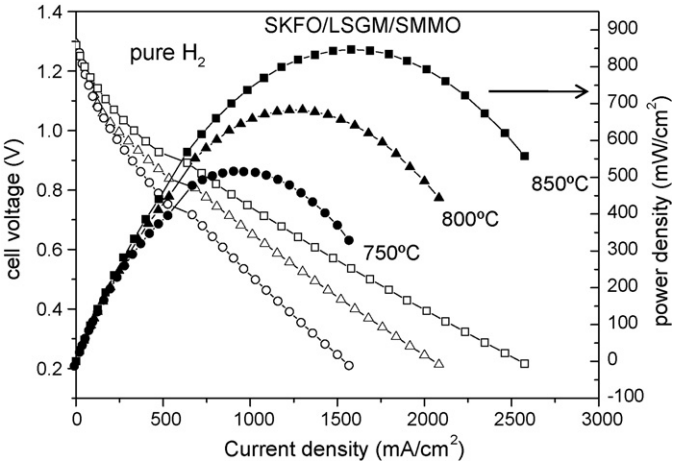

Fig. 3. Cell voltage (left axis) and power density (right axis) as a function of the current density for the test cell with $Sr_{0.9}K_{0.1}FeO_{3-\delta}$ as a cathodic material.

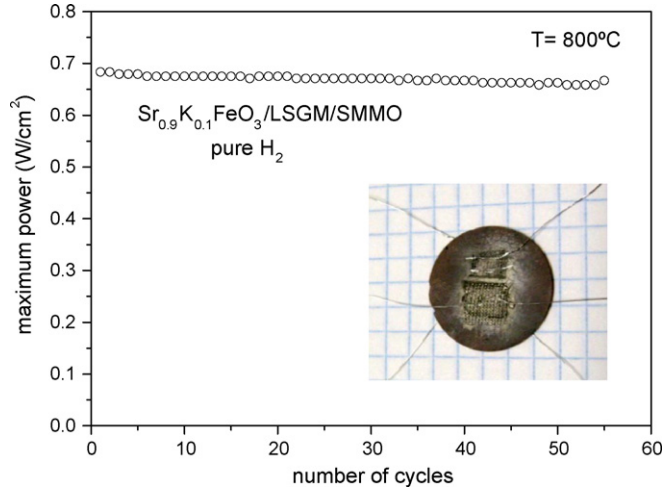

Fig. 4. Stability of the test cell with $Sr_{0.9}K_{0.1}FeO_{3-\delta}$ as a cathodic material at 800 °C *vs* the cycle number. Inset: aspect of the electrolyte supported cell, view from the cathodic side.

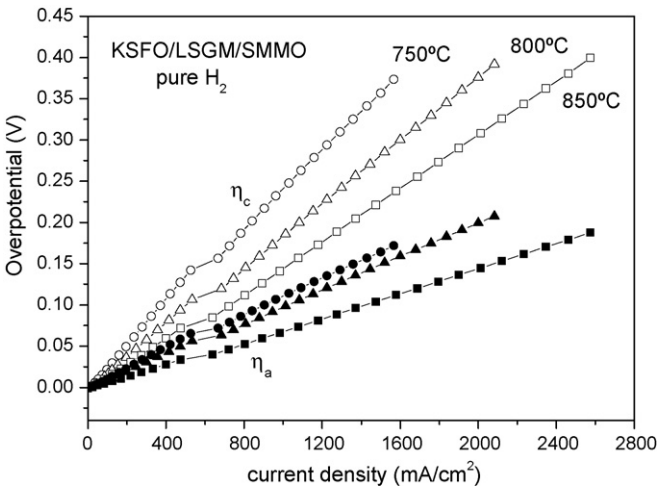

Fig. 5. Anodic and cathodic overpotentials for test cells with $Sr_{0.9}K_{0.1}FeO_{3-\delta}$ as a cathodic material.

the single cell operating at the three mentioned temperatures are compared in Fig. 5. The dependences of η_a and η_c on the current density agree well with that of the power density. Very remarkably, η_c takes significantly low values; for instance, η_c is below 0.1 V for a current density of 500 mA cm^{-2}. The influence of Pt paste on the performance of the electrodes was addressed in preceding works by the same group (e.g. Ref. [8]): even without Pt paste, with buried Pt mesh into the electrodes, the performance of the cell did not significantly decrease.

Fig. 6 shows a representative micrograph of the cross section of the cathodic side of the test cell. It shows clear interfaces of the $Sr_{0.9}K_{0.1}FeO_{3-\delta}$ (SKFO) cathode and the electrolyte $La_{0.8}Sr_{0.2}Ga_{0.83}Mg_{0.17}O_{3-\delta}$ (LSGM) after testing in H_2. From the SEM image, the thickness of SKFO is about 30 μm. Its grain and particle size vary from 1 to 2 μm. Moreover, the cathode SKFO exhibits a fine and uniform microstructure with an estimated 30% porosity.

The described test-cell shows a non-negligible power of 680 mW cm^{-2} at 800 °C, surpassing the requirements of 500 mW cm^{-2} at 800 °C for practical use of a single cell. It also exhibits a good cyclability without apparent power loss up to 50 cycles. Moreover, the cathodic overpotential takes small values, below 0.1 V at a current density of 500 mA cm^{-2} at 800 °C, and therefore the cathodic losses are no longer rate-determining for

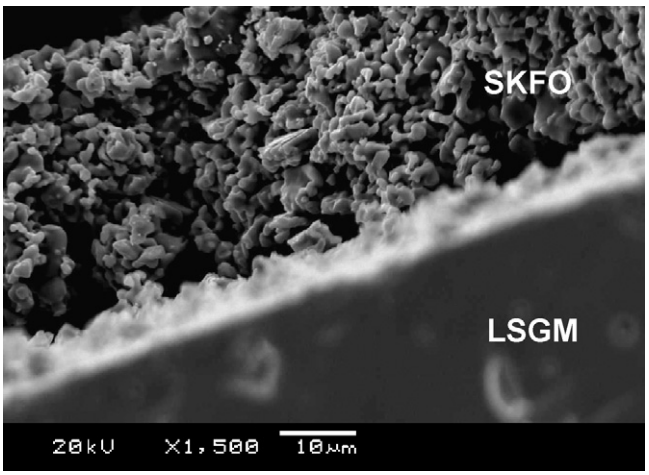

Fig. 6. SEM image of a cross section of the test cell with $Sr_{0.9}K_{0.1}FeO_{3-\delta}$ (SKFO) as a cathodic material and $La_{0.8}Sr_{0.2}Ga_{0.83}Mg_{0.17}O_{3-\delta}$ (LSGM) as electrolyte.

the output power of the cell. The ohmic loss across the electrolyte is now rate limiting, since the electrode overpotentials are not likely to be rate limiting at those current densities with H_2 fuel and thick-film electrodes. So, it seems that a way to improve the performance would be to make these cells either anode- or cathode-supported, thus reducing the thickness of the electrolyte to a minimum value.

We can correlate the observed performance with some structural aspects of the perovskite phase constituting the major component of the cathode material. The $Sr_{0.9}K_{0.1}FeO_{3-\delta}$ oxide exhibits, at room temperature, a tetragonal structure characterized by the absence of tilting of the FeO_6 octahedra (Fe–O–Fe = 180°), which ensures a maximum overlap between Fe 3*d* and O 2*p* orbitals, and thus accounts for an enhanced conductivity in the low-temperature regime by electronic hopping via Fe–O–Fe paths. The electronic conductivity shows a change of regime at $T \approx 350\,^{\circ}C$ that could correspond to the phase transition from tetragonal to cubic symmetry. The high-temperature regime is characterized by metallic behavior.

The second important structural feature observed from thermal analysis data is the significant oxygen deficiency exhibited at high temperatures: the crystal structure contains 0.20(1) oxygen vacancies per formula unit randomly distributed over the oxygen sites (if a cubic symmetry is assumed) at 800 °C. The presence of disordered vacancies could account, by itself, for the oxide-ion conductivity that is required for the mass transport across the cathode. On the other hand, the observed porosity of the cathode material (Fig. 6) also contributes to the diffusion and transport of oxygen into the electrode to contact a larger surface area. The final step of the reduction of O_2 to $2O^{2-}$ that is transferred to the anode through the electrolyte requires the surface transfer of oxygen from the reaction site on the $Sr_{0.9}K_{0.1}FeO_{3-\delta}$ surface to the electrolyte.

The variable-valence $SrFeO_{3-\delta}$ ($0.0 \leq \delta \leq 0.5$) perovskites system is a paradigmatic example of the influence of the oxygen content and the order–disordering phenomenon on the magnetic and electronic properties of an oxide material. One of the end members, $SrFeO_{2.5}$, exhibits a brownmillerite structure where the oxygen vacancies are long-range ordered, giving rise to alternate planes of tetrahedrally and octahedrally oxygen-coordinated Fe cations [13]. In this compound the Fe^{3+} cations exhibit a localized $3d^5$ configuration so that the compound is an antiferromagnetic Mott-type insulator. The other end member, the cubic perovskite $SrFeO_3$, exhibits the coexistence of metallic conductivity ($\rho \approx 10^3\,S\,cm^{-1}$ at 300 K) [14,15] and screw-type antiferromagnetic ordering ($T_N \approx 130$ K) [16]. This unusual combination of metallic conductivity and antiferromagnetism in $SrFeO_3$ reflects a localized π-bonding t^3 configuration coexisting with itinerant σ-bonding electrons of e-orbital parentage as a result of the enhanced Fe–O covalency [17–19]. By Mössbauer spectroscopy, high-spin electronic configurations have been determined for the Fe^{4+} d^4 and Fe^{3+} d^5 cations present in the end members of the series [13,20]. The oxygen-stoichiometric $SrFeO_3$ perovskite can only be stabilized under high oxygen pressure [3,21]. Under the usual preparation conditions, in air at ambient pressure, oxygen-defective perovskites with intermediate oxygen contents are realized. Typically, oxygen contents between 2.74 and 2.91 per formula unit are obtained by annealing the samples in air at temperatures around 800–1000 °C [21]. The $SrFeO_{2.5}$ brownmillerite requires reducing conditions, e.g. by annealing in an H_2/Ar flow. Different vacancy-ordered perovskite structures have been identified for the intermediate members $Sr_4Fe_4O_{11}$ ($SrFeO_{2.75}$) and $Sr_8Fe_8O_{23}$ ($SrFeO_{2.875}$) [21,22]. For both of these compositions, a semiconductive behavior has been reported [23,24]. Nearly metallic conduction with $\rho \approx 10^{-3}\,\Omega\cdot cm$ was observed in the polycrystalline perovskite $SrFeO_{2.92}$. The temperature coefficient of resistivity $d\rho/dT$, however, was negative down to 12 K, indicating that the material is not truly metallic [23]. The presence of oxygen vacancies opens an energy gap between localized Fe d^4 and itinerant d^5L^{-1} states, leading to an activated behavior, whereas in the fully stoichiometric $SrFeO_{3.0}$ perovskite, pinning of the Fe(V)/Fe(IV) redox couple at the top of the O 2p bands leads to a metallic ground state [25].

In $Sr_{0.9}K_{0.1}FeO_{3-\delta}$, on the other hand, we have retained a metallic temperature dependence of the conductivity in the presence of a substantial number of oxygen vacancies at the working temperature of a fuel cell to obtain an ideal MIEC behavior. The introduction of K has a twofold effect: on the one hand, the larger ionic radius of K^+ (1.64 Å [26]) with respect to Sr^{2+} (1.44 Å) combined with the hole-doping effect induces an increase of the tolerance factor, favoring the stabilization of an untilted crystal structure with Fe–O–Fe angles of 180°, which maximizes the Fe–O–Fe interactions. On the other hand, the presence the K would boost the Fe valence to promote an adequate ionic conductivity at the working temperature.

4. Conclusions

In conclusion, we have designed, characterized, and tested a K-doped $SrFeO_{3-\delta}$ perovskite as a cathode material for intermediate-temperature SOFCs with long-term stability and competitive power performance in the temperature range 750–850 °C. The Fe^{4+} of $SrFeO_3$ is reduced to Fe^{3+} by oxygen loss at the operating temperature of an intermediate-temperature SOFC. The introduction of K^+ at the Sr^{2+} sublattice partially reoxidizes Fe^{3+} to Fe^{4+}, improves the O 2p bandwidth, and leads to a good electronic conductivity at the working temperature range 750–850 °C. The result is a competitive cathode material containing no cobalt that meets the target for the intermediate-temperature SOFC.

Acknowledgements

We are grateful to ILL for making the beamtime available. JBG thanks the NSF and to Robert A. Welch Foundation of Houston, TX, for financial support. JAA acknowledges the financial support of the Spanish "Ministerio de Ciencia e Innovación" to the project MAT2007-60536 and during his sabbatical.

References

[1] L.-W. Tai, et al., Solid State Ionics 76 (1995) 273.
[2] L.-W. Tai, M.M. Nasrallah, H.O. Anderson, J. Solid State Chem. 118 (1995) 117.
[3] Y. Takeda, K. Kanno, T. Takada, O. Yamamoto, M. Takano, N. Nakayama, Y. Bando, J. Solid State Chem. 63 (1986) 237.
[4] J. Mizusaki, M. Okayasu, S. Yamauchi, K. Fueki, J. Solid State Chem. 99 (1992) 166.
[5] M.L. Post, B.W. Sanders, P. Kennepohl, Sens. Actuators B 13–14 (1993) 272.
[6] J.J. Tunney, M.L. Post, J. Electroceram. (2005) 63.
[7] J.J. Tunney, M.L. Post, X. Du, D. Yang, J. Electrochem. Soc. 149 (2002) H113.
[8] Y.-H. Huang, R.I. Dass, Z.-L. Xing, J.B. Goodenough, Science 312 (2006) 254.
[9] J.B. Goodenough, Y.H. Huang, J. Power Sources 173 (2007) 1.
[10] H.M. Rietveld, J. Appl. Crystallogr. 2 (1969) 65.
[11] J. Rodríguez-Carvajal, Physica B 192 (1993) 55.
[12] S.E. Dann, M.T. Weller, D.B. Currie, M.F. Thomas, A.D. Al Rawwas, J. Mater. Chem. 3 (1993) 1231.
[13] P.K. Gallagher, J.B. MacChesney, D.N.E. Buchanan, J. Chem. Phys. 41 (1964) 2429.
[14] J.B. MacChesney, R.C. Sherwood, J.F. Potter, J. Chem. Phys. 43 (1965) 1907.
[15] T. Takeda, H. Watanabe, J. Phys. Soc. Jpn. 33 (1972) 973.
[16] T. Takeda, Y. Yamaguchi, H. Watanabe, J. Phys. Soc. Jpn. 33 (1972) 967.
[17] H. Adachi, M. Takano, J. Solid State Chem. 93 (1991) 556.
[18] A.E. Bouquet, A. Fujimori, T. Mizokawa, T. Saitoh, H. Nagatame, S. Suga, N. Kimizuki, Y. Takeda, M. Takano, Phys. Rev. B 45 (1992) 1561.
[19] M. Abbate, F.M.F. de Groot, J.C. Fuggle, A. Fujimori, Q. Strebel, F. Lopez, M. Domke, G. Kaindl, G.A. Sawatzky, M. Takano, Y. Takeda, Phys. Rev. B 45 (1992) 1561.
[20] M. Takano, J. Kawachi, N. Nakanishi, Y. Takeda, J. Solid State Chem. 39 (1981) 75.

[21] H. Falcón, J.A. Barbero, J.A. Alonso, M.J. Martínez-Lope, J.L.G. Fierro, Chem. Mater. 14 (2002) 2325.
[22] J.P. Hodges, S. Short, J.D. Jorgensen, X. Xiong, B. Dabrowski, S.M. Mini, C.W. Kimball, J. Solid State Chem. 151 (2000) 190.
[23] S. Nakamura, S. Iida, Jpn. J. Appl. Phys. 34 (1995) L291.
[24] J. Hombo, Y. Matsumoto, T. Kawano, J. Solid State Chem. 84 (1990) 138.
[25] P. Adler, A.F. Goncharov, K. Syassen, Hyp. Int. 95 (1995) 71.
[26] R.D. Shannon, Acta Cryst. A 32 (1976) 751.